Estimation of the zone of excavation disturbance around tunnels, using resistivity and acoustic tomography

Koichi Suzuki[1] Eiji Nakata[1] Masayuki Minami[2] Etsuhisa Hibino[2] Tomonori Tani[3]
Jyunichi Sakakibara[4] Naoyuki Yamada[5]

Key Words: resistivity tomography, acoustic tomography, excavation disturbance, tunnel

ABSTRACT

The objective of this study is to estimate the distribution of a zone disturbed by excavation (EDZ) around tunnels that have been excavated at about 500 m depth in pre-Tertiary hard sedimentary rock. One of the most important tasks is to evaluate changes in the dynamic stability and permeability of the rock around the tunnels, by investigating the properties of the rock after the excavation.

We performed resistivity and acoustic tomography using two boreholes, 5 m in length, drilled horizontally from the wall of a tunnel in pre-Tertiary hard conglomerate. By these methods, we detected a low-resistivity and low-velocity zone 1 m in thickness around the wall of the tunnel. The resulting profiles were verified by permeability and evaporation tests performed at the same boreholes. This anomalous zone matched a high-permeability zone caused by open fractures.

Next, we performed resistivity monitoring along annular survey lines in a tunnel excavated in pre-Tertiary hard shale by a tunnel-boring machine (TBM). We detected anomalous zones in 2D resistivity profiles surrounding the tunnel. A low-resistivity zone 1 m in thickness was detected around the tunnel when one year had passed after the excavation. However, two years later, the resistivity around the tunnel had increased in a portion, about 30 cm in thickness, of this zone. To investigate this change, we studied the relationship between groundwater flow from the surroundings and evaporation from the wall around the tunnel. These features were verified by the relationship between the resistivity and porosity of rocks obtained by laboratory tests on core samples. Furthermore, the profiles matched well with highly permeable zones detected by permeability and evaporation tests at a horizontal borehole drilled near the survey line. We conclude that the anomalous zones in these profiles indicate the EDZ around the tunnel.

[1] Central Research Institute of Electric Power Industry
     1646 Abiko, Abiko-shi, Chiba, Japan, 270-1194
     Tel: +81-4-7182-1181
     Fax: +81-4-7183-3182
     Email: k-suzuki@criepi.denken.or.jp

[2] Tokyo Electric Power Company
     1-1-3 Uchisaiwai, Chiyoda-ku, Tokyo, Japan, 100-0011

[3] Tokyo Electric Power Service Co. Ltd
     3-3-3 HigashiUeno, Daito-ku, Tokyo, Japan, 100-0015

[4] JFE Civil Engineering & Construction Corp
     2-17-4 Kuramae, Daito-ku, Tokyo, Japan, 100-0051

[5] Dia Consultants Co. Ltd.
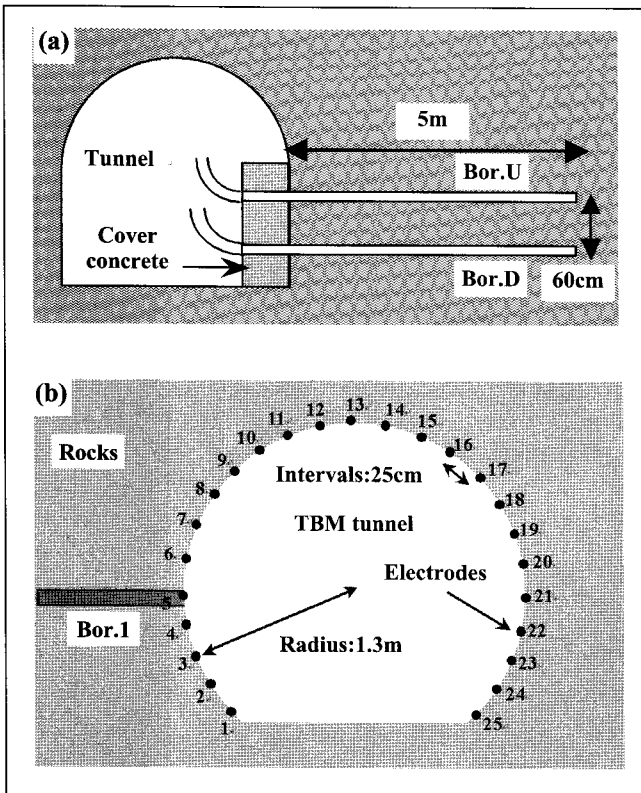   2-272-3 Yoshino, Saitama-shi, Saitama, Japan, 330-8660

INTRODUCTION

In the excavation of underground tunnels, it is important to estimate the dynamic stability and hydraulic permeability of the rock around the tunnels by investigating physical response. There are some case studies that investigate the zone disturbed by excavation (EDZ), which results from stress redistribution during excavation, and subsequent rock re-equilibration. For example, Ninomiya et al. (1989) imaged the EDZ using seismic tomography before and after excavation. Kuwahara et al. (1995) delineated the EDZ using seismic, resistivity, and electromagnetic wave tomography, and estimated the change of water content in the rocks. Bossart et al. (2002) investigated the EDZ, finding open fractures around a tunnel in Jurassic sedimentary rocks. The geophysical methods in these studies have provided images of the distribution of resistivity and seismic velocity around tunnels. However, there are more practical physical properties of the EDZ that are important from an engineering point of view. Few studies have estimated the relationship between resistivity and seismic velocity, or physical properties of the EDZ that are of interest to engineers.

The purpose of our study is to evaluate the EDZ around tunnels by estimating physical properties of importance to engineers from profiles obtained by geophysical exploration. To do this, we have conducted acoustic and resistivity tomography using two boreholes drilled horizontally from the wall of a tunnel, and a resistivity survey with an annular survey line around the wall of a TBM tunnel. We compared the conclusions from geophysical exploration of the EDZ with the results of hydraulic permeability and evaporation tests using the same boreholes, and laboratory tests using core samples.

OUTLINE OF THE SITES

The sites are located in tunnels excavated about 500 m deep in a mountainous area. Site A is in a hard Cretaceous sedimentary formation, consisting of coarse-grained sandstones and conglomerate. The boreholes used for the acoustic and resistivity tomography were 5 m long, and separated by 60 cm (Figure 1a). Site B is in a TBM tunnel 2.6 m in diameter, located in Cretaceous sedimentary rocks containing chert and shale. We performed an electrical survey on an annular line around the tunnel (Figure 1b).

MEASUREMENTS AND METHODS OF ANALYSIS

(1) Acoustic tomography

This method was used to image the geophysical structure between the two boreholes at site A. We installed pipes at the head of each borehole head to fill the boreholes with water (Figure 1a), and used a piezoelectric transmitter and multiple hydrophones as receivers. Measurement points were spaced at a 10-cm interval between 0 and 2 m from the surface, and at a 20-cm interval between 2 and 4 m. The frequencies of the transmitted signal were 15 kHz, 31 kHz, and 78 kHz.

Fig. 1. (a) Layout of boreholes at site A. (b) Position of electrodes and borehole Bor.1 at site B.
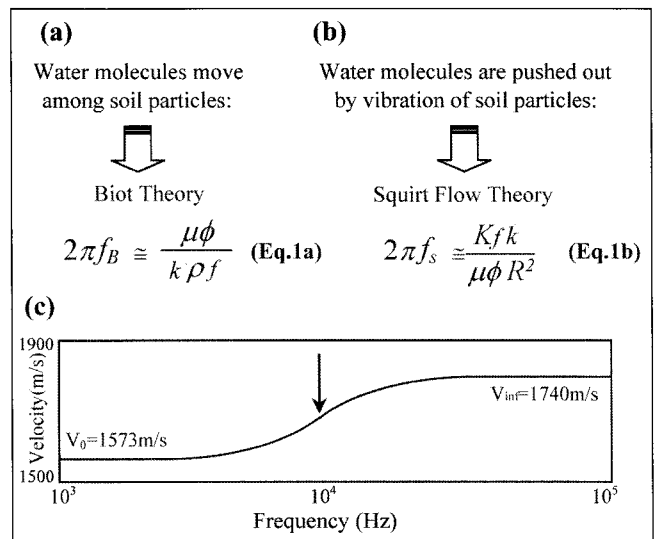

Fig. 2. Concept of the BISQ model (Dvorkin et al., 1993). (a) Biot theory for soft sedimentary rocks. (b) Squirt flow theory for hard rocks. Here k is hydraulic conductivity, f_B is the frequency at the inflection point of the velocity/frequency curve, by Biot theory, f_S is the frequency at the inflection point of the velocity/frequency curve, by Squirt flow theory, ϕ is rock porosity, ρ_f is fluid density, K_f is the modulus of elasticity of the fluid, R is a characteristic length of Squirt flow, and μ is fluid viscosity. (c) Variation with frequency of elastic acoustic wave velocity of rocks.

We used the BISQ model (Dvorkin and Nur, 1993) to analyse 2D acoustic wave velocity, attenuation profiles, and porosity and hydraulic conductivity profiles. This model combines Biot's theory (Biot, 1956) and Squirt flow theory (Dvorkin et al., 1995), as shown in Figures 2a and 2b, and is suitable for hard sedimentary rocks as are found at this site. The physical properties, porosity and hydraulic conductivity, can be derived by determining the frequency of the inflection point in the velocity-frequency curve (Figure 2c).

(2) Resistivity tomography and electrical survey

At site A, electrodes were placed at the same points as used for acoustic tomography. We measured resistivity data using the pole-pole array. The distance between the remote electrodes and the boreholes was about 100 m.

At site B, electrodes were placed along the annular survey line around the tunnel wall. Twenty-five electrodes were installed 25 cm apart along the line (Figure 1b). We pasted non-polarization electrodes consisting of conductive gel, made by Oyo Co., directly on the wall. Resistivity data were measured using the dipole-dipole array. The maximum interval between current and potential dipoles was 250 cm. We repeated the experiment three times, acquiring data sets one year, two years, and three years after the excavation.

An alternating current at 0.4 s period was transmitted by the CRIEPI data acquisition system (Suzuki et al., 1992). Resistivity data were analysed with a 2D resistivity inversion scheme, which consists of smoothness-constrained least-squares optimisation and an algorithm for the rapid calculation of partial derivatives (Sasaki, 1988). In the two-dimensional inversion, we treated the wall of the tunnel as a ground surface with severe topography.

(3) Electrical logs

At site B, an electrical log was obtained in borehole Bor.1, which was drilled horizontally 1 m above the floor and 1 m away from the electrical survey line. The length of the borehole was 2 m. Apparent resistivity was measured using the Wenner array. The electrode spacing was 10 cm.

(4) Permeability and evaporation tests

Permeability and evaporation tests were performed by installing a mechanical double packer system with 10-cm interval (minimum) in the boreholes at site A and site B that were used for geotomography and electrical logs. The objective was to obtain permeability profiles along the small diameter radial boreholes that were drilled into the EDZ (Bossart et al., 2002). The length of the interval enclosed by the packer was 10 cm (at depths of 0.0–1.0 m from the wall), 20 cm (1.0–2.0 m), and 50 cm (2.0–5.0 m). The evaporation test was performed by observing injection of dry air into the test interval, or extraction of air out of the EDZ using a vacuum pump. After the evaporation test, the permeability test was conducted by injecting water into the test interval and recording the resulting changes in water flow rate and pressure.

The principal specifications of the instruments used are shown in Table 1.

INTERPRETATION OF FIELD DATA

(1) Site A

Acoustic wave velocity and attenuation cross-sections are shown in Figures 3a and 3b. The horizontal axis shows distance from the surface of the 40-cm thick concrete wall covering. The velocity ranges from 4.2 km/s to 4.9 km/s, which is within acceptable limits for pre-Tertiary hard sediments. The region to a depth of 1 m from the wall exhibits lower velocity. Attenuation ranges from 0.08 to 0.4 dB/m/kHz. The edges of the cross-section display high attenuation because of air left in the boreholes.
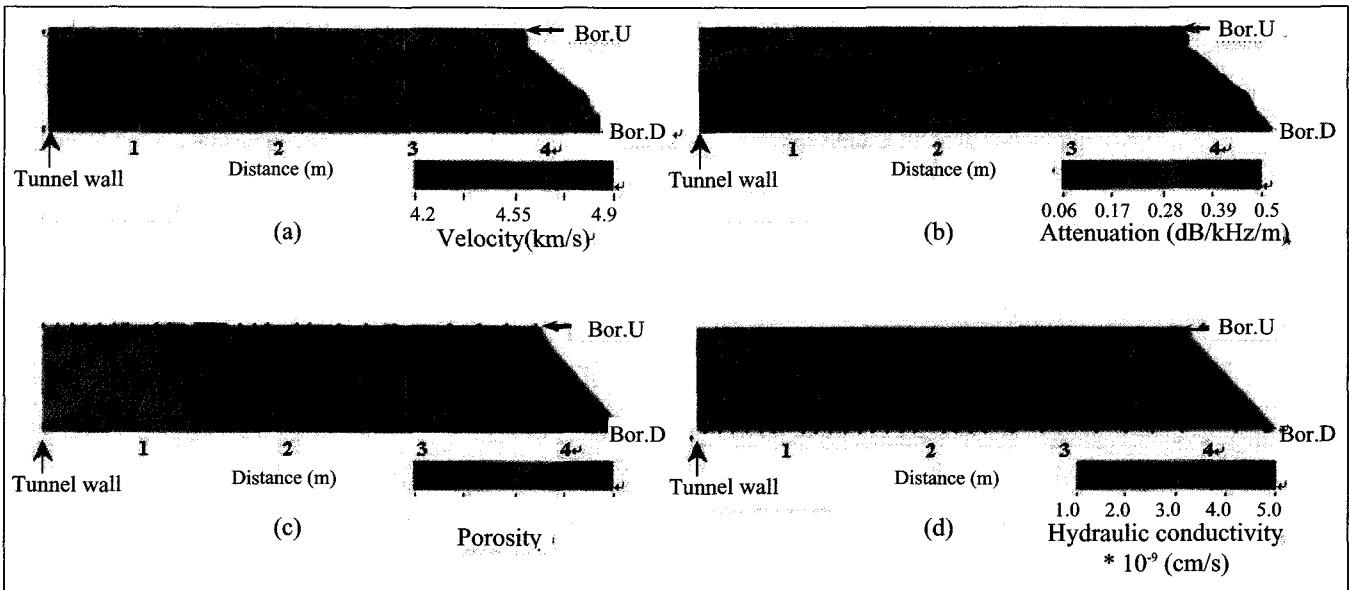
Fig. 3. Velocity, attenuation, porosity, and permeability cross-sections based on acoustic tomography.

Porosity and hydraulic conductivity cross-sections are shown in Figures 3c and 3d. The porosity ranges from 0.02 to 0.15. High porosities are found in the zone to a depth of 1 m from the wall. Hydraulic conductivity is of the order of 10^{-9} cm/s, and is higher near the wall than at greater depths. A resistivity cross-section is shown in Figure 4. The resistivity ranges from 100 to 5000 Ω.m, and a low-resistivity zone appears near the wall.

We compare the results of permeability and evaporation tests (Figures 5a and 5b) in Bor. U (Tani et al., 2002) with the geophysical cross-sections (Figures 5c and 5d). In the zone 50 cm deep from the rock surface, indicated by the rectangular dotted
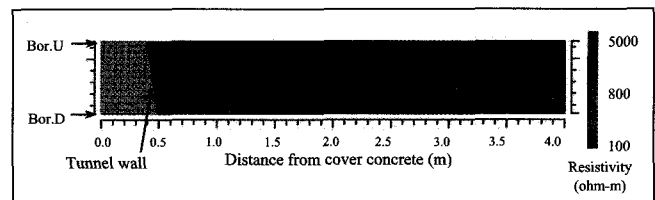
Acoustic Tomography	
Piezoelectric transmitter	$\varnothing$ 44 mm × 1200 mm (ITC Co.)
Receiver	$\varnothing$ 20 mm × 24 channels
	(Kawatetu Co.)
Computer	4ch (Pentium 800)
FFT Analyzer	Onosokki co.

Resistivity Tomography	
Resistivity Meter	McOhm-21 (Oyo Co.)
	Voltage: 400V p-p; Current:
	1–200 mA
	Frequency: 3.5 sec.
	Accuracy 20 μV
Borehole electrodes	20ch. 10 cm interval (Ask system)

Electrical survey (CRIEPI)	
Transmitter mA	Voltage: 400V p-p; Current: 1-800
	Frequency: 0.2–1.6 sec.
Receiver	Gain: -30dB-60dB; A/D: 12 bit
Electrode Selector	60ch. For 4-electrodes
Computer	Epson PC-286LE
Electrodes	Geo-gel non-polarizing type
	(Oyo Co.)

Electrical Log	
Resistivity Meter	Mini-ohm (Oyo Co.)
	Current: 10 μA–1 mA
Cable	4ch; Electrodes: 10 cm interval

Table 1. Principal specifications of instruments used.

Fig. 4. Resistivity cross-section from resistivity tomography.

line, the hydraulic conductivity is very high, in the range of 10^{-7}–10^{-5} cm/s. We also compare the fracture distribution in both boreholes (Bor. U and Bor. D), as shown in Figure 5e, with the geophysical profiles. We recognize that the highly fractured area near the wall coincides with part of the low-velocity and low-resistivity zone within the rectangular dotted line.

The amount of evaporation near the wall is also higher than at greater depths. Therefore, we conclude that the fractures in this zone are open, which would account for the low velocity and low resistivity in the zone marked by the rectangular dotted line in Figure 5. The arrows in Figures 5b, 5c, and 5d indicate where low-velocity and low-resistivity features appear to correspond to other fractures, marked by red circles in Figure 5e, observed in the boreholes.

(2) Site B

Resistivity cross-sections measured one, two, and three years after the excavation are shown in Figures 6a, 6b, and 6c. The position of the borehole (Bor.1) is projected onto the cross-sections. The resistivity ranges from 300 to 3980 Ω.m. A low-resistivity zone (300–500 Ω.m) about 1 m thick was observed around the tunnel when one year had passed after excavation, as shown in Figure 6a. Two and three years after excavation, a layer about 30 cm thick of this low-resistivity zone had changed to high resistivity (1500–2000 Ω.m) as shown in Figures 6b and 6c.

A resistivity change $\Delta\rho$ is calculated as follows:

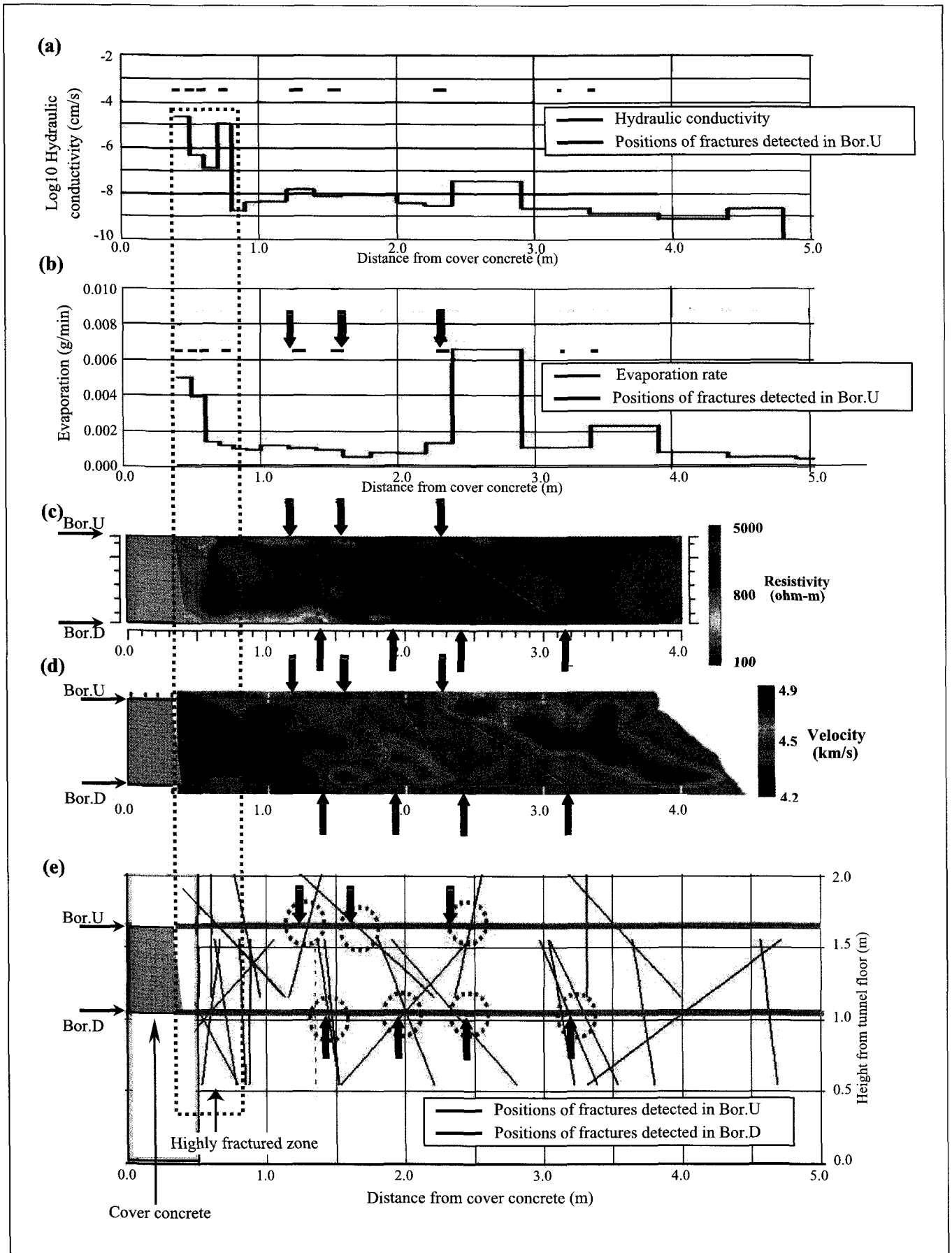$$\Delta\rho = (\rho_a - \rho_b)/\rho_b , \tag{1}$$

Fig. 5. Comparison of permeability, evaporation tests, geotomography cross-sections, and fracture distribution. Red arrows indicate the positions of fractures detected in the boreholes. (a) Results of permeability tests at Bor.U. (b) Results of evaporation tests at Bor.U. (c) Resistivity cross-section from resistivity tomography. (d) Velocity cross-section from acoustic tomography. (e) Fracture observations in Bor.U and Bor.D.
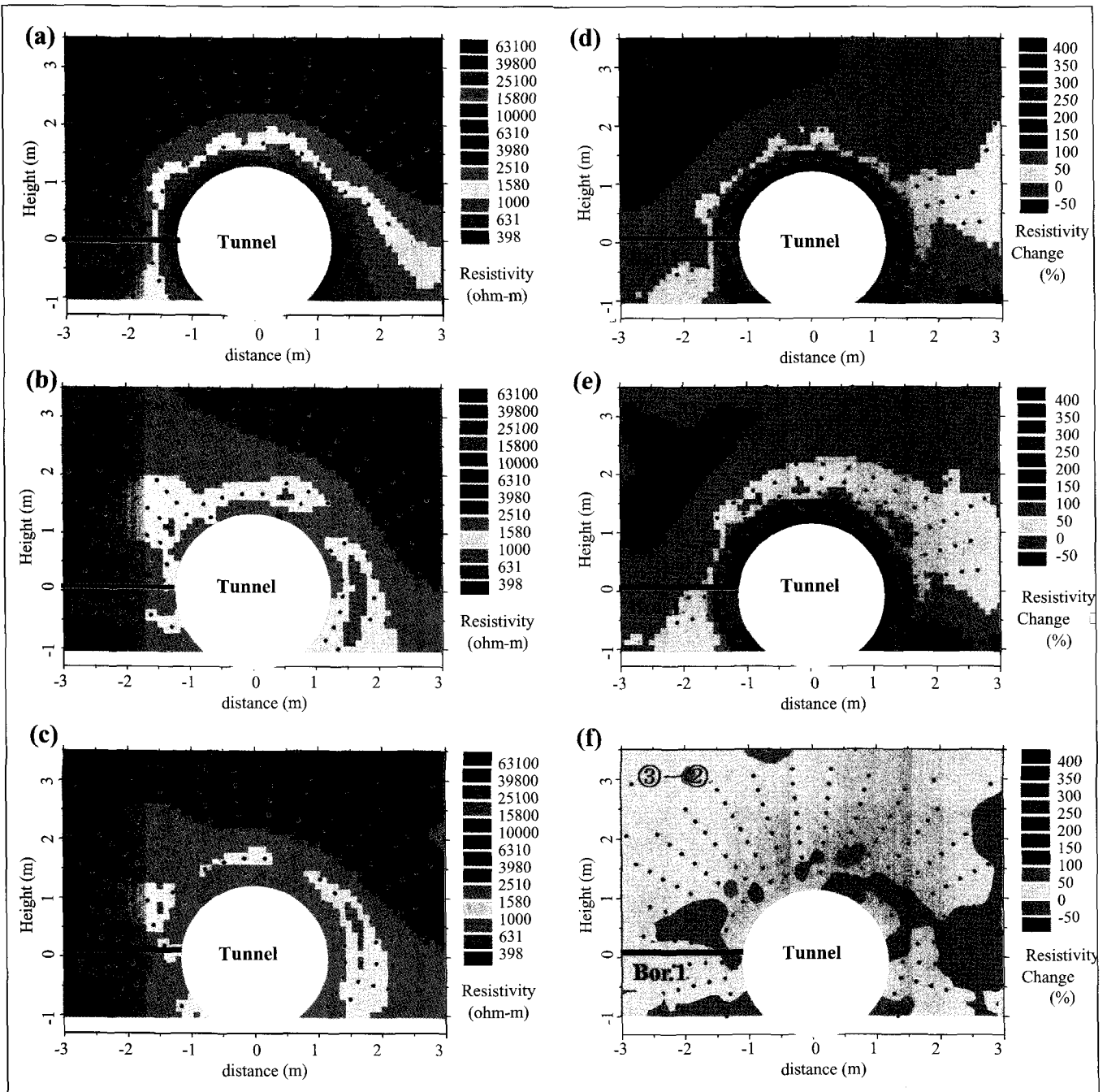
Fig. 6. Resistivity cross-sections at site B. (a) Resistivity cross-section one year after excavation. (b) Resistivity cross-section two years after excavation. c) Resistivity cross-section three years after excavation. (d) Cross-section of resistivity change between resistivity cross-sections (a) and (b). (e) Cross-section of resistivity change between resistivity cross-sections (a) and (c). (f) Cross-section of resistivity change between resistivity cross-sections (a) and (c).

where ρ_b is the resistivity measured one year after the excavation, ρ_a is the resistivity measured one or two years later. A cross-section showing resistivity change between one year and two years, shown in Figure 6d, clearly indicates the annular high-variation zone (200–400%) around the tunnel wall. The cross-section showing resistivity change between one year and three years (Figure 6e) also indicates the occurrence of the high-variation zone clearly, but there is no clear zone of change in Figure 6f, which shows the changes that occurred between two and three years after excavation.

In order to investigate these resistivity variations, we conducted electrical logging, permeability and evaporation tests at Borehole Bor.1, and laboratory tests using core samples. The resistivity logging data indicate that the zone 1 m deep from the wall exhibits resistivity

of 1500–2000 Ω.m, while deeper zones show 2000–3000 Ω.m (Figure 7a). The former corresponds to a highly fractured area, with fractures being shown by arrow symbols in Figure 7a. We conducted permeability and evaporation tests in the same borehole after three years had passed since the excavation, with results shown in Figures 7b and 7c. Within the first 30 cm from the wall, the hydraulic conductivity is high, over 10^5 cm/s. The amount of evaporation near the wall is also higher than in other zones. We conclude that the zones of high resistivity change in Figures 6d and 6e are also zones of high hydraulic conductivity and high evaporation rate.

LABORATORY TESTS

The results of laboratory tests using core samples are shown in Figure 8. Eight core samples were cut to columns of 20 mm in
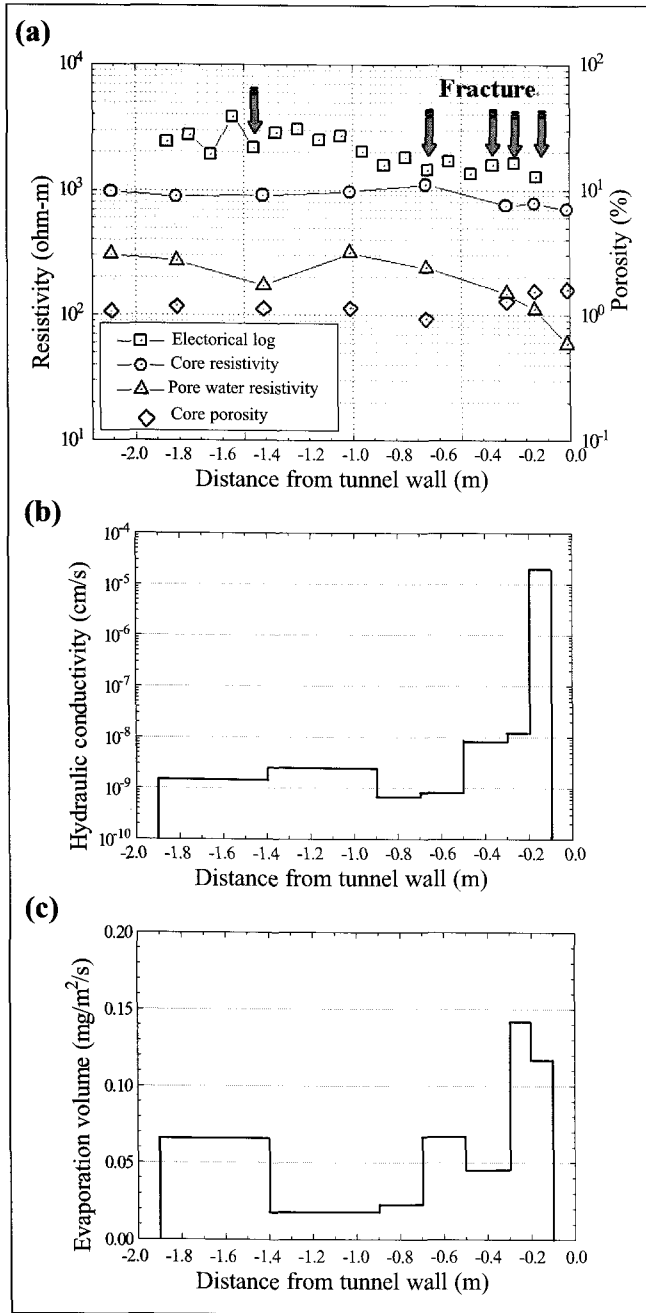
Fig. 7. Results of electrical logs, permeability tests, and evaporation tests at site B. (a) Electrical log resistivity, sample resistivities, sample pore water resistivities, and sample porosities. (b) Permeability test in Bor.1. (c) Evaporation test in Bor.1.

length and 98 mm in diameter. The description of each sample is shown in Table 2. We followed the procedure for resistivity measurement described in Chiba and Kumada (1994). Initially, each sample was placed in an individual container with 300 ml of distilled water, and held under vacuum for two days. We then measured the resistivity of each water and core sample. Each sample was then dried for two days, and placed under vacuum for two days while immersed in a KCl solution. This step was repeated with KCl solutions of eight different concentrations (20, 200, 2000, 5000, 10 000, 15 000, 20 000, and 32 500 ppm). We assumed that the resistivity of the fluid in which the sample was saturated was equal to that of pore water in each sample, and measured the resistivity of each sample and solution at each of the concentrations. The resistivity of the solutions was measured with a B173 conduction meter made by Horiba.
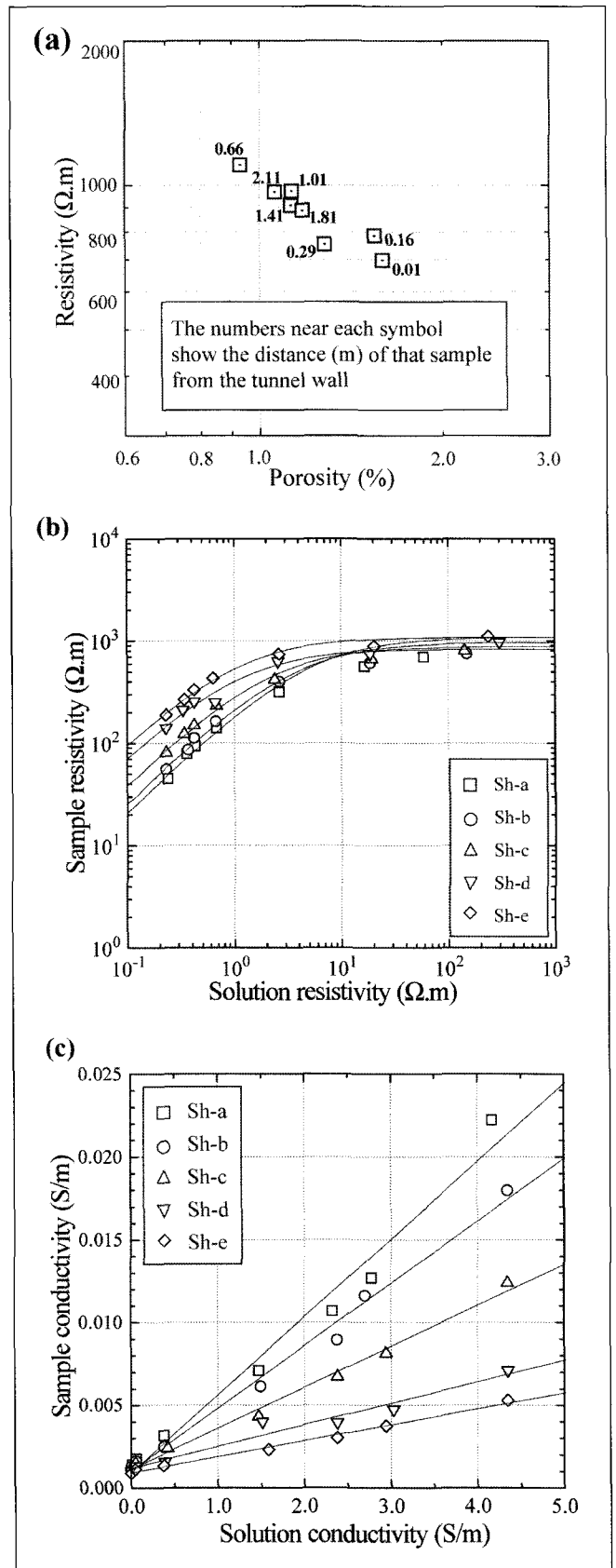

Fig. 8. Results of laboratory tests on core samples. (a) Porosity versus resistivity. (b) Solution resistivity versus sample resistivity. (c) Solution conductivity versus sample conductivity. The explanation of the legend is in Table 2.

The porosity ϕ was calculated from

$$\phi = (w_a - w_d)/(w_a - w_w), \quad (2)$$

where w_a is the fully saturated weight of the sample in air, w_w is the fully saturated weight in water, and w_d is the dry weight in air. Each dry weight was measured after drying for 5 days at 60°C. The resistivity of core samples fully saturated with distilled water ranges from 600 to 1000 Ω.m, which is lower than reported by electrical logging data (Figure 7a). The difference may be explained as follows: either the rock at site B was partially saturated, or the pore water content of the samples was higher than that in situ, because of increased porosity caused by stress release. The resistivity of the pore water is in the range 60–300 Ω.m, and the sample from near the wall surface exhibits lower resistivity than those from greater depth (Table 2). The relationship between porosity and resistivity is shown in Figure 8a. The porosity range is 0.9–1.7%, and the sample from near the wall shows higher porosity than do the others. Consequently, there is a negative correlation between the porosity and resistivity of the samples.

To investigate the relationship between KCl solution resistivity ρ_w and sample resistivity ρ_R, the measured values were plotted as shown in Figure 8b, in which the horizontal axis is ρ_w and the vertical axis is ρ_b. The symbols show measured values, and the solid lines are theoretical curves explained below.

Katsube and Hume (1983) proposed that bulk surface conduction occurred on pore surfaces in rocks, in addition to conduction through pore water, and derived the equations

$$\frac{1}{\rho_R} = \frac{1}{F\rho_w} + \frac{1}{\rho_c}, \quad (3a)$$

and

$$F = a\phi^{-m}, \quad (3b)$$

where ρ_R is the resistivity of the rock, ρ_w is the resistivity of the pore water, ϕ is the effective porosity, a and m are empirical constants depending on the type of rock, ρ_c is the bulk surface

Depth (cm)	Density (g/cm³)	Porosity (%)	Formation Factor	ρc (Ω.m)	Symbol
0–2	2.66	1.59	214	1071	Sh-a
15–17	2.70	1.55	256	862	Sh-c
28–30	2.70	1.28	263	990	Sh-b
65–67	2.69	0.93	1025	1085	Sh-e
100–102	2.70	1.13	885	877	
140–142	2.70	1.13	990	909	
180–182	2.69	1.18	735	901	
210–212	2.70	1.06	763	980	Sh-d

Table 2. Description of rock samples.

resistivity, and F is known as the formation factor. Equation (3) can be rewritten in terms of conductance as

$$\sigma_R = \frac{1}{F}\sigma_w + \sigma_c. \quad (3c)$$

Equation (3c) plots as a straight line in σ_w–σ_R coordinates, where σ_w is pore water conductivity and σ_R is sample conductivity. Therefore, we can evaluate the formation factor (F) and the bulk surface resistivity (ρ_c) by calculating a linear regression line.

The estimated values of F and ρ_c are shown in Table 2. The measured values match well to the theoretical curves calculated from equation 3a (Figure 8b) and equation 3c (Figure 8c). When ρ_w is less than 1.0 Ω.m, the measured values are accounted for by Archie's law (Archie, 1942). However, if rw is greater than 10 Ω.m, ρ_R becomes constant and is independent of ρ_w.

DISCUSSION

A decrease in resistivity of the rock can occur for the following reasons, assuming that the rock remains saturated with groundwater flow into the area surrounding the tunnel: either the pore water content of the rock has increased, because fracture apertures, or porosity in the rock matrix, has increased due to relaxation of the rock after excavation; or the salinity of the pore water is increased by evaporation from the tunnel wall. On the other hand, the factors leading to an increase in resistivity of the rock might be: either the water content of the rock has decreased, because the porosity of the rocks has decreased; or the amount of groundwater flow from undisturbed ground into the area surrounding of the tunnel has decreased, again reducing the water content of the rocks.
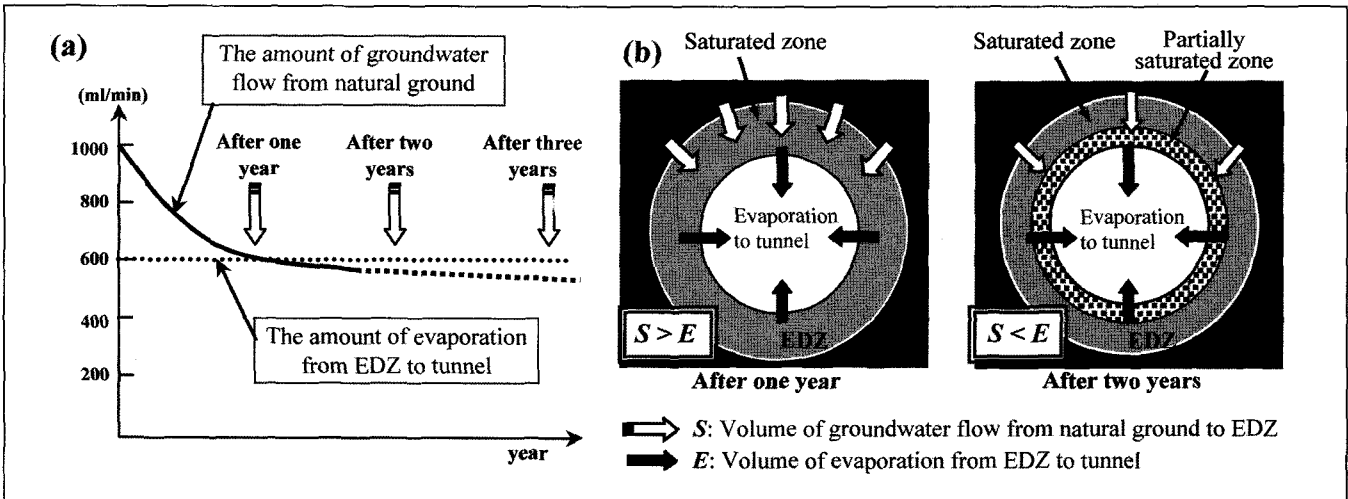

Fig. 9. Groundwater flow model suggested by resistivity observations, and the water flow from the tunnel. (a) The change of the total amount of water flow from the tunnel, measured at the tunnel entrance. (b) Model showing the amount of groundwater flow from undisturbed rock to the EDZ and the amount of evaporation from the EDZ through the wall to the tunnel.

At site A, the low-velocity zone detected by acoustic tomography, which is at a depth of about 1 m from the wall of the tunnel, is consistent with the highly fractured zone interpreted as a water flow path. Therefore, we consider that this zone, which is imaged as a low-velocity zone in the cross-section, corresponds to the EDZ. In contrast, the low-resistivity zone found by resistivity tomography, which is at a depth of about 20 cm from the wall, does not coincide well with the low-velocity zone. We consider that the resistivity in a portion of the low-velocity zone has been increased by a reduced level of saturation, which has been estimated by permeability and evaporation tests (Tani et al., 2002).

At site B, a low-resistivity zone was evident one year after the excavation, and had disappeared a year later (Figures 6a and 6b). We propose the following sequence (Figure 9) as one of several possible scenarios. One year after excavation, fracture aperture or porosity in the rocks to a depth of about 1 m from the tunnel wall has increased, because of rock stress relaxation following the excavation, and the water content in the rock has also increased by groundwater flow from undisturbed rock into the area surrounding the tunnel. As a result, the resistivity of this zone has decreased. This interpretation is consistent with the laboratory tests (Figure 8a). In addition, salinity of the groundwater could have increased because of evaporation from the wall. This is supported by the observation that the pore water resistivity is low in cores near the wall (Figure 7a) and the relationship between pore water resistivity and rock resistivity (Figure 8b). Two and three years after the excavation, the amount of groundwater flow from undisturbed ground has fallen, to be lower than the amount of evaporation from the wall. Consequently, the surface rocks have become unsaturated, and the resistivity of the area within 30 cm of the tunnel wall has increased gradually with decreasing water content.

This interpretation agrees well with the results of permeability and evaporation tests at borehole Bor.1, because the zone at a depth of about 30 cm around the tunnel is interpreted to be highly permeable. The interpretation also agrees with the change in the total amount of water flowing from the tunnel wall, measured at the entrance of the tunnel, which decreased gradually after excavation as shown in Figure 9a. We suggest that during the first year after excavation, the rocks surrounding the tunnel were fully saturated, because the amount of groundwater flow from undisturbed rock was higher than that of evaporation from the tunnel wall. After the first year, as the amount of the groundwater flow became less than that of evaporation, rocks around the wall gradually changed to being partially saturated (Figure 9b).

CONCLUSIONS

The 2D acoustic and resistivity tomography cross sections have enabled us to visualize the EDZ around tunnels in pre-Tertiary sedimentary rock. Resistivity measurements were also effective in monitoring groundwater flow and the effect of evaporation in the EDZ after the excavation. Time-lapse resistivity measurements can be a useful tool in visualizing changes in water saturation.

REFERENCES

Archie, G. E., 1942, The electrical resistivity log as an aid in determining some reservoir characteristics: *Trans. A.I.M.E.*, **146**, 56–67.

Biot, M.A., 1956, Generalized theory of acoustic propagation in porous dissipative media: *The Journal of the Acoustical Society of America*, **34**, 1634–1645.

Bossart P., Peter M.M., Moeri A., Trick T., and Mayor J., 2002, Geological and hydraulic characterisation of the excavation disturbed zone in the Opalinus Clay of the Mont Terri Rock Laboratory: *Engineering Geology*, **66**, 19-38.

Chiba, A., and Kumada, M., 1994, Resistivity measurement for granite and tuff samples. - Influence of pore water fluid resistivity on rock resistivity: *BUTSURI-TANSA (Geophysical Exploration)*, **47**, 161–172.

Dvorkin, J., and Nur, A., 1993, Dynamic poroelasticity: unified model with the squirt and Biot mechanisms: *Geophysics*, **58**, 524–553.

Dvorkin, J., Mavko, G., and Nur, A., 1995, Squirt flow fully saturated rocks: *Geophysics*, **60**, 97–107.

Katsube, T.J., and Hume, J.P., 1983, Electrical resistivities of rocks from Chalk River: *Proceeding of Geophysical Geoscience Research at Chalk River*, 105–114.

Kuwahara, T., Ueno, T., Kaneda, Y., Suzuki, K., Namiki, M., Hirama, K., Tamai, S., and Nagai, K., 1995, Evaluation of rocks in large-scale caverns using geotomography methods (2), - analysis of caverns and estimation of excavation disturbed zone using seismic, electromagnetic wave, and resistivity: *Ohbayashi technical report*, **51**, 33–38.

Ninomiya, Y., Sugihara, H., Ito, K., Kamemura, K., and Aoki, T., 1989, Evaluation of excavation disturbed zone around caverns using geotomography methods: *Proceedings of the 21st Symposium on Rock Mechanics (Japanese Society of Civil Engineers)*, 151–155.

Sasaki, Y., 1988, Improved Two-Dimensional resistivity inversion: *BUTSURI-TANSA (Geophysical Exploration)*, **41**, 111–115.

Suzuki, K., Jyomori, N., and Azuma, Y., 1992, Development of automatic data acquisition instruments for resistivity method: *Proceedings of the 87th SEGJ Conference*, 161–164.

Tani, T., Iketani, S., Oyama, T., Minami, M., and Hibino, K., 2002, Evaluation of hydraulic properties of rocks around caverns using permeability and evaporation tests in short sections, *Proceeding of the 32nd Symposium on Rock Mechanics (Japanese Society of Civil Engineers)*, 1–8.